PERGAMON

International Journal of Solids and Structures 36 (1999) 4333–4361

INTERNATIONAL JOURNAL OF SOLIDS and STRUCTURES

Stress concentrations in composites with interface sliding, matrix stiffness and uneven fiber spacing using shear lag theory

Chad M. Landis*, Robert M. McMeeking

Department of Mechanical and Environmental Engineering, University of California, Santa Barbara, CA 93106, U.S.A.

Received 26 February 1998; in revised form 10 June 1998

Abstract

The stress concentrations near a single fiber break in a unidirectionally reinforced fiber composite are investigated using a shear lag theory within the framework of finite elements. A model for uniformly spaced, well bonded fibers embedded in a matrix that cannot carry axial loads that was formulated previously is first introduced. The solution of this problem involves Fourier transforms and requires only a two-dimensional numerical integration. The work described in the current paper characterizes the stress concentrations around a single fiber break in the presence of fiber/matrix interface sliding, axial matrix stiffness and uneven fiber spacing. Due to the introduction of these complicating factors, the model no longer lends itself to the simple Fourier transformation solution method. For the case of interface sliding a new method is developed to handle sliding in any shear lag system. For the cases of axial matrix stiffness and uneven fiber spacing a finite element code specifically written for this problem is used to determine the fiber stresses. The results are discussed in the context of global versus local load sharing, and the effects on composite failure.

1. Introduction

The failure of a unidirectionally reinforced fiber composite material is a complex event. Initially all fibers are intact and able to carry load. As increasing load is applied to the composite, the weakest fiber will eventually fail. The loads that are shed by the broken fiber near the failure site must then be transferred to other fibers and possibly to the matrix. Exactly where and how much of the load is transferred depends on many parameters. The strength and sliding resistance of the fiber/matrix interface, the fiber to matrix moduli ratio, the matrix cracking or yield stress and the regularity of the fiber spacing are just a few of these parameters.

* Corresponding author. Tel: 001 805 893 7833; Fax: 001 805 893 8651; E-mail: landis@engineering.ucsb.edu

0020-7683/99/$ - see front matter
PII: S0020-7683(98)00193-0

After the first break occurs, the load is redistributed and this can cause other fibers to fail and thus shed further load to intact fibers. At some point the composite as a whole will be unable to carry additional load and failure will ensue. The failure of the composite can fall between the extremes of Global Load Sharing (GLS) on the one hand and nearest neighbor Local Load Sharing (LLS) on the other. GLS is associated with a material where fiber breaks do not cause stress concentrations in the other intact fibers and the stress along a broken fiber recovers to the applied stress linearly from the break. As will be discussed later, this type of load transfer requires sliding along the fiber/matrix interface and a relatively stiff matrix. A GLS composite with a large number of fibers will have a stress-strain behavior that is initially linear, then as fibers progressively fail the material will soften until a smooth maximum in the stress is reached (Curtin, 1991; Hui et al., 1995).

Composites that undergo brittle failure, where the material behaves nearly linear elastically up to fracture, are usually associated with what has been termed Local Load Sharing (LLS). In a LLS material intact fibers experience a stress concentration in the presence of a break. Fibers closest to the break will experience the highest stress concentration. In the extreme case, only nearest neighbors experience the stress concentration and other fibers further from the break are unaffected. This is associated with what has been termed a local load sharing rule. This type of local load sharing does not actually happen in most physical systems. In general, stress concentrations are distributed throughout the system. The magnitude of these stress concentrations and how they depend on features of the composite system is the topic of this paper.

Due to the very complicated three-dimensional nature of composite materials, finite element modeling is perhaps the best candidate for investigating the detailed stress distributions in the fibers and matrix. Unfortunately, to investigate a composite of any significant size and to account for the effects of all of the parameters mentioned above would require extensive amounts of computation time. To alleviate this problem, shear lag models have become a common feature in composite microstress analysis. Shear lag is a term used to describe a model that represents a three-dimensional structure, such as a fiber, as a one-dimensional axial load carrying entity. Other assumptions common to shear lag models include that the matrix cannot carry any axial loads, the fibers are well bonded to the matrix, the fibers are arranged in a uniformly spaced array, and the fibers are only allowed to displace along their axis. The model presented here is able to relax all of these assumptions, although we do use the assumption of allowing only axial displacements for simplicity.

The shear lag concept was introduced by Cox (1952). His analysis only considered the stresses along a single broken fiber in an elastic matrix and other neighboring fibers were not directly included in the model. Since then shear lag models have been used to investigate the stresses along a broken fiber in the presence of different matrix constitutive behaviors. Du and McMeeking (1995) formulated a model for a creeping matrix, and Landis and McMeeking (1998) solved the governing shear lag equation for a perfectly plastic matrix with deformation governed by J_2 flow theory. Landis and McMeeking (1998) also give an overview of the various models along with a model that includes both elastic load recovery and constant shear stress sliding at the fiber/matrix interface. Since these models do not directly include neighboring fibers the stress concentrations in the unbroken fibers are not determined. This deficiency has been the primary shortcoming of these models.

Hedgepeth (1961) and Hedgepeth and van Dyke (1967) formulated shear lag models that predict

stresses in an infinite array of fibers. The three dimensional model of Hedgepeth and van Dyke (1967) was improved upon by Landis et al. (1998) such that the model directly includes next nearest neighbor interactions and the stiffness of the matrix springs that connect the fibers can be explicitly related to matrix material properties. The basic assumptions of these shear lag models are that the fibers can be represented by one-dimensional axial springs and that the matrix transfers load between fibers via shear stress but does not carry any axial load itself. These models also assume that the fibers are well bonded to the matrix and the fibers are arranged in an evenly spaced array. These shear lag models yield what is termed an influence function which requires a numerical integration to evaluate the stress at any position on any fiber in the composite.

Today's materials processing methods rarely produce a perfect array of fibers. Slip along the fiber/matrix interface is sometimes desired and designed into the material, and the effect of matrix stiffness is most pronounced in systems with fiber to matrix moduli ratios near unity. So how do stress concentrations vary as these parameters are taken into account? We have formulated a new method to model sliding in any shear lag system and use it to investigate the effect of sliding on stress concentrations. We will also use a finite element model proposed by Cox et al. (1994) that represents fibers as one dimensional axial springs and the matrix as three dimensional finite elements to investigate how the stress concentrations vary near a single break for the cases of axial matrix stiffness and uneven fiber spacing. Interface sliding, axial matrix stiffness, and uneven fiber spacing will each be considered separately. We have assumed the absence of residual stresses, but these could be included by using simple superposition constructions.

2. Well bonded fibers in a matrix without axial stiffness

This problem has been solved by Landis et al. (1998), but we will summarize the results since this problem is closely related to other cases and its solution is required for the sliding model. The formulation is identical to that of Hedgepeth and van Dyke (1967) except in the treatment of the matrix. We also note that this formulation is the continuous form of the finite element model proposed by Cox et al. (1994). First consider the segment of finite element mesh drawn in Fig. 1. The complete mesh extends out infinitely in all directions repeating the cell shown. The black dot is a representative node in the mesh, and all of the other nodes and elements that influence the equilibrium of this central node are included in the drawing. The equation governing the displacement of this node is identical to the equation governing the displacement of any other node in the system. The dark lines represent fiber elements, and the 'bricks' are matrix elements.

Each node is allowed to displace only along the fiber direction, x, as shown in Fig. 1. The fiber elements are one-dimensional springs between nodes with stiffness $E_f A_f/\Delta x$ where E_f is the Young's modulus of the fibers, A_f is the cross sectional area of the fibers, and Δx is the distance between nodes as shown in Fig. 1. The matrix element is assumed to have no axial stiffness, i.e. $E_m = 0$, but a finite shear modulus G_m. This assumption has been interpreted as being representative of a matrix that has failed in tension due to cracking or yielding at a low stress. Each matrix element is essentially a system of springs connecting each node to all other nodes in the element. The stiffness of each of these springs is determined by the finite element method, see Cook et al. (1974). The stiffnesses for the 3D brick elements shown in Fig. 1 are given in Appendix A. Note that the

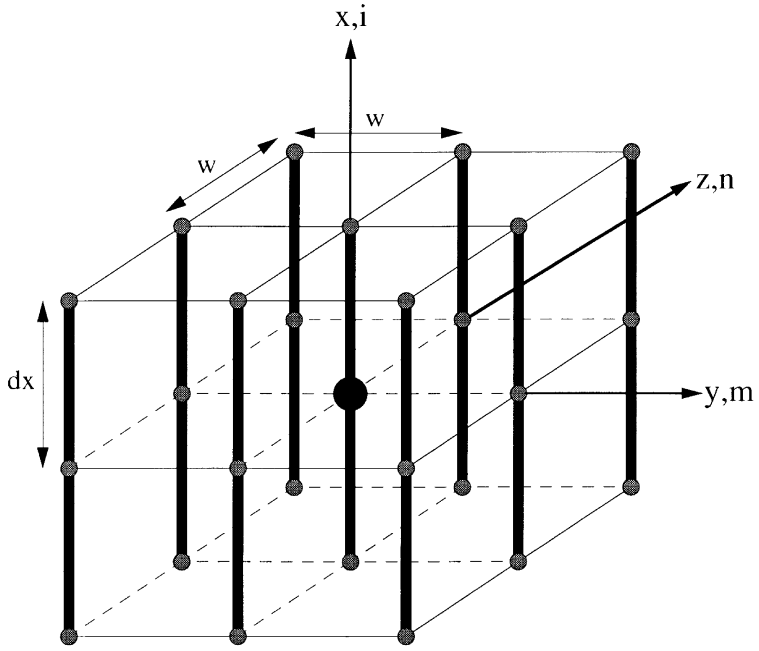

Fig. 1. The black circle is a representative node in the finite element mesh. The mesh drawn includes all of the nodes and elements that affect the equilibrium of the central node. The dark lines represent one dimensional fiber elements, and the 'bricks' with dimensions $w \times w \times \Delta x$ are three-dimensional brick elements with matrix properties.

expressions for the stiffnesses contain E_{m}, but for this problem the matrix has no axial stiffness, i.e. $E_{\mathrm{m}} = 0$.

Once all of the stiffness terms are known for each element then the stiffness matrix of the 27 node cell of Fig. 1 can be assembled. The equation governing the displacement of the central node is then the general form of the equation governing any other nodal displacement in the system. It is now possible to make this system continuous in the x-direction by taking the limit as Δx goes to zero. In this limit the finite element equations governing the displacements of the nodes are transformed to ordinary differential equations governing the displacement distributions along the fibers. The equation governing the x displacement, $U_{\mathrm{m,n}}$, of a fiber located at position m, n in the square lattice is

$$\frac{\mathrm{d}^2 U_{m,n}}{\mathrm{d}x^2} + \frac{4}{3\pi}(U_{m+1,n+1} + U_{m+1,n} + U_{m+1,n-1} + U_{m,n+1} + U_{m,n-1} + U_{m-1,n+1} + U_{m-1,n} + U_{m-1,n-1} - 8U_{m,n}) = 0 \quad (1)$$

where D is the fiber diameter and is related to the fiber cross sectional area by $A_{\mathrm{f}} = \pi D^2/4$. Note that m and n can take on any integer values, and thus eqn (1) represents an infinite set of equations. Following the procedure originated by Hedgepeth and van Dyke (1967) this set of equations can be solved using a Fourier transformation and influence function technique. Consider the problem where a central fiber, $m = 0$ and $n = 0$, is broken at $x = 0$, under far field applied strain, ε. The

solution is obtained by superposing the solution for an applied strain of $-\varepsilon$ at $x = 0$ on fiber $(m = 0, n = 0)$, termed the 'auxiliary problem', and the trivial uniform strain solution. The boundary conditions for the auxiliary problem are:

$$\frac{\mathrm{d}U_{0,0}}{\mathrm{d}x}(x = 0) = -\varepsilon \tag{2a}$$

$$U_{m,n}(x = 0) = 0 \quad \text{for} \quad m,n \neq 0,0 \tag{2b}$$

$$U_{m,n}(x = \infty) = 0 \quad \text{for} \quad \text{all } m \text{ and } n \tag{2c}$$

Then the stress, $\sigma_{m,n}$, at any x-position, in the fiber located at site m, n in the lattice for the central break problem, is given by

$$\frac{\sigma_{m,n}(\xi)}{E_{\mathrm{f}}\varepsilon} = 1 + q_{m,n}(\xi) \tag{3}$$

where

$$\xi = \sqrt{\frac{4}{3\pi}}\sqrt{\frac{G_{\mathrm{m}}}{E_{\mathrm{f}}}}\frac{x}{D} \tag{4}$$

and

$$q_{m,n}(\xi) = \frac{-\int_0^{\pi}\int_0^{\pi} \cos n\theta \cos m\phi(\alpha \exp\left[-\alpha|\xi|\right])\mathrm{d}\theta\mathrm{d}\phi}{\int_0^{\pi}\int_0^{\pi} \alpha \mathrm{d}\theta\mathrm{d}\phi} \tag{5}$$

with

$$\alpha = \sqrt{8 - 2\cos\theta - 2\cos\phi - 4\cos\theta\cos\phi} \tag{6}$$

Note that the absolute value in eqn (5) arises due to the fact that $q_{m,n}(-\xi) = q_{m,n}(\xi)$. Also, $q_{m,n}$ is the solution for the normalized stresses in the fibers for the auxiliary problem. The result for the stress concentration factor in a nearest neighbor fiber is 1.081. Landis et al. (1998) have pointed out that this value for the maximum stress concentration in a nearest neighbor fiber is in much better agreement with more detailed finite element calculations done by Nedele and Wisnom (1994) ($SCF \approx 1.06$–1.07) than the earlier shear lag model of Hedgepeth and van Dyke (1967) ($SCF = 1.14$). Note that the magnitudes of the stresses do not depend on the moduli ratio, but in contrast the length scale over which stresses are perturbed do depend on this ratio. For example, a composite with a very compliant matrix will have elevated stresses in a fiber next to a break over much longer distances than a composite with a very stiff matrix. This becomes a very important feature when the statistics of fiber failure are considered. A fiber that has a high stress acting over a given length will have a higher probability of failure than a similar fiber with the same stress magnitude acting over a shorter length. Equations (3)–(6) are the solution for a 'perfect' composite in which the fiber/matrix interface is well bonded, the matrix has zero axial stiffness and the fibers

are arranged in a perfectly square lattice. The power of this technique is that it gives the stress at any fiber position in the composite (i.e. for any m, n and ξ). Furthermore, the influence function given in eqns (5) and (6) can be used along with superposition techniques to compute the stresses in the composite when there are multiple, arbitrarily located breaks as has been done with a two-dimensional influence function by Sastry and Phoenix (1993) and Beyerlein and Phoenix (1997).

3. Sliding at the fiber/matrix interface

In this section we will determine the stress concentration in a fiber adjacent to a broken one in the presence of sliding at the fiber/matrix interface. First we will present the closed form solution of sliding in single fiber shear lag models to illustrate the problem. The first single fiber shear lag model was presented by Cox (1952) and Nairn (1997) has recently improved upon the original model. Landis and McMeeking (1998) have presented the following model for interface sliding. A literature search has been carried out to determine whether this model has been developed elsewhere, but no such work was found.

All single fiber shear lag models that assume the matrix behaves elastically have a solution for a break at $x = 0$ of the following general form:

$$\frac{\sigma}{E_f \varepsilon} = \frac{du}{d\xi} = 1 - \exp\left[-|\xi|\right] \tag{7}$$

$$\hat{\tau} = -\frac{d^2 u}{d\xi^2} - \mathrm{sgn}(\xi)\exp\left[-|\xi|\right] \tag{8}$$

where

$$\xi = C_1 \sqrt{\frac{G_m}{E_f}}\frac{x}{D}, \quad u = C_1 \sqrt{\frac{G_m}{E_f}}\frac{1}{\varepsilon}\frac{U}{D}, \quad \hat{\tau} = C_2 \sqrt{\frac{E_f}{G_m}}\frac{\tau}{E_f \varepsilon} \tag{9a–c}$$

where x is the axial coordinate along the fiber, U is the axial displacement, σ is the axial stress, τ is the shear stress acting at the fiber surface and the function sgn (ξ) is equal to 1 if $\xi \geqslant 0^+$ or -1 if $\xi \leqslant 0^-$. The constants C_1 and C_2 are chosen to be consistent with eqns (7) and (8) and can depend on the geometry of the system and the elastic properties of the fiber and matrix. Note that the constants C_1 and C_2 will be different for the Cox (1952) and Nairn (1997) models, but that the general form of eqns (7)–(9) remains unchanged.

In order to introduce sliding, we must assume some constitutive behavior for the fiber/matrix interface. In metal matrices with strong fiber/matrix interfaces, sliding is governed by shear yielding of the matrix. In many ceramic and titanium matrix composites there is no strong chemical bond between the fiber and matrix and stresses at the fiber matrix interface are governed by frictional sliding in ceramic matrices or yielding of a fiber coating in titanium matrices. Polymer matrix composites tend to have a strong fiber/matrix bond and therefore the sliding process in polymer matrix composites is a more complicated fracture phenomenon. The actual debonding of the interface is governed by energy release rates and subsequent sliding of a fiber segment is governed by friction. In order to capture most of these features we will use a simple interface constitutive

model described by Beyerlein and Phoenix (1996) in which a region of the interface along the fiber will first debond when the magnitude of the shear stress at that position is equal to a critical debonding stress τ_D. Once the fiber has debonded it will slide along the matrix with a constant sliding stress τ_0. The solution for sliding in a single fiber takes the form

$$\frac{\sigma}{E_f\varepsilon} = \hat{\tau}_0|\xi|, \quad \hat{\tau} = -\operatorname{sgn}(\xi)\hat{\tau}_0 \tag{10a–b}$$

in the sliding zone, $-\hat{L}_s \leqslant \xi \leqslant \hat{L}$, where $\hat{L}_s$ is

$$\hat{L_s} = C_1\sqrt{\frac{G_m}{E_f}}\frac{L_s}{D} \tag{11}$$

and L_s is the length from the break to the end of the sliding zone. Outside of the sliding zone where $|\xi| > \hat{L}_s$, the stresses take the form

$$\frac{\sigma}{E_f\varepsilon} = 1 - C\exp[-|\xi|], \quad \hat{\tau} = -\operatorname{sgn}(\xi)C\exp[-|\xi|] \tag{12a–b}$$

The constant C and the sliding zone length $\hat{L}_s$ are determined by applying the following boundary conditions. At the end of the sliding zone, $\xi = \hat{L}_s$, the axial stress must be continuous and the normalized shear stress must be equal to $-\hat{\tau}_0$ for the values of ξ infinitesimally less than $\hat{L}_s$ and $-\hat{\tau}_D$ for values of ξ infinitesimally greater than $\hat{L}_s$. The complete solution to this problem is then

$$\frac{\sigma}{E_f\varepsilon} = \begin{cases} \hat{\tau}_0|\xi| & \text{for} \quad |\xi| \leqslant \hat{L_s} \\ 1 - \hat{\tau}_D\exp[\hat{L_s} - |\xi|] & \text{for} \quad |\xi| > \hat{L_s} \end{cases},$$

$$\hat{\tau} = \begin{cases} -\operatorname{sgn}(\xi)\hat{\tau}_0 & \text{for} \quad |\xi| < \hat{L_s} \\ -\operatorname{sgn}(\xi)\hat{\tau}_D\exp[\hat{L_s} - |\xi|] & \text{for} \quad |\xi| > \hat{L_s} \end{cases}, \quad \hat{L_s} = \frac{1}{\hat{\tau}_0} - \frac{\hat{\tau}_D}{\hat{\tau}_0} \tag{13a–c}$$

Note that $\sigma(-\xi) = \sigma(\xi)$ and $\tau(-\xi) = -\tau(\xi)$. As demonstrated here, the solution to the sliding problem requires matching the sliding and elastic solutions at $\hat{L}_s$.

Considering the solution to the single fiber shear lag model with sliding, it is useful to investigate the form of the elastic solutions for multi-fiber shear lag models. The general form of the governing equations for a multi-fiber shear lag model is

$$\frac{d^2u_i}{d\xi_2} + \sum_{j=1}^{N} A_{ij}\frac{du_j}{d\xi} + \sum_{j=1}^{N} B_{ij}u_j = 0 \quad \text{for} \quad i = 1 \quad \text{to} \quad N \tag{14}$$

where u_i are normalized axial or transverse displacements of a fiber or region of matrix and N is the number of fiber and matrix regions multiplied by the number of displacements allowed per region (i.e. 3 if axial and transverse displacements are allowed). We choose the normalizations represented by u, ξ and $\hat{\tau}$ such that

$$\frac{\sigma_i}{E_{f,m}\varepsilon} = \frac{du_i}{d\xi} \quad \text{and} \quad \hat{\tau}_i = -\frac{d^2u_i}{d\xi^2},$$

where $E_{f,m}$ denotes the fiber or matrix Young's modulus depending on whether i represents a fiber

or matrix region. Note here that the numbering system has changed from that used in eqns (1) and (5). In this numbering scheme each fiber or matrix region is specified by a single number instead of an ordered pair as in eqns (1) and (5). This is more useful when a finite number of regions are considered, but the ordered pair scheme must be used for infinite composites. In our models the A_{ij} and B_{ij} are determined by the finite element method in the same manner described in the previous section for the 'perfect' composite. Equation (14) can represent a shear lag system with axial matrix stiffness, random fiber spacing and transverse displacements. The solution to eqn (14) can be obtained in a variety of ways. If $N \to \infty$ and the material has a periodic geometry then the Fourier series transformation of the previous section must be used. For finite N, numerical methods (as in the next sections) or the characterization of the appropriate eigensystem can be used as the solution procedure. In general, with a far field strain of ε applied to the system, the axial stress along fiber or matrix region i with a single break at $\xi = 0$ in fiber or matrix region j is

$$\frac{\sigma_i(\xi)}{E_{f,m}\varepsilon} = 1 + q_{ij}(\xi) \tag{15}$$

where ξ is again a normalized coordinate along the fiber and $q_{ij}(\xi)$ is the influence function which gives the strain at ξ on line of freedom i due to the presence of a normalized unit opening *load* at $\xi = 0$ on line of freedom j. Again, $E_{\mathrm{f,m}}$ is equal to the fiber or matrix Young's modulus if i is a fiber or matrix line of freedom respectively. The influence function, q_{ij}, can take the form of an integral as in eqn (5), a series of exponential functions if the eigensystem solution method is used, or a list of tabulated values if a numerical solution procedure is implemented.

Now that we know the form of the elastic solutions for our shear lag systems the problem becomes one of matching the sliding solution to the elastic solution. To do this we will first discuss the Break Influence Superposition (BIS) technique developed by Sastry and Phoenix (1993). Consider an elastic shear lag system consisting of a matrix and fibers with M arbitrarily loaded breaks as shown in Fig. 2. Define Λ_{ij} to be the strain at break i due to a unit opening load at break j. Note that the Λ_{ij} can contain interactions between both fiber and matrix failure sites. Therefore, this definition of Λ_{ij} is slightly different from that used in Sastry and Phoenix (1993) which only considered interactions of fiber breaks. Let w_j be a weight given to break j. Note that w_j is proportional to the opening displacement of break j. Then the traction on break i, p_i, is given by

$$\frac{p_i}{E_{\mathrm{f,m}}\varepsilon} = \sum_{j=1}^{M} \Lambda_{ij} w_j \tag{16}$$

If we desire the solution for a uniform traction on all breaks with zero far field applied strain then we set all of the $p_i = -E_{\mathrm{f,m}}\varepsilon$ and solve the set of equations given by eqn (16) for the weights, w_j. Once this solution is obtained then the uniform strain field ε is superposed to obtain the solution for traction free breaks with a uniform strain applied at infinity. The stress at any point in the composite is then

$$\frac{\sigma_i(\xi)}{E_{\mathrm{f,m}}\varepsilon} = 1 + \sum_{j=1}^{M} q_{ij}(\xi - \xi_j) w_j \tag{17}$$

where $\sigma_i(\xi)$ is the stress at ξ along line of freedom i, q_{ij} is the influence function for line of freedom i due to a unit opening load on line of freedom j and ξ_j is the axial location of break j.

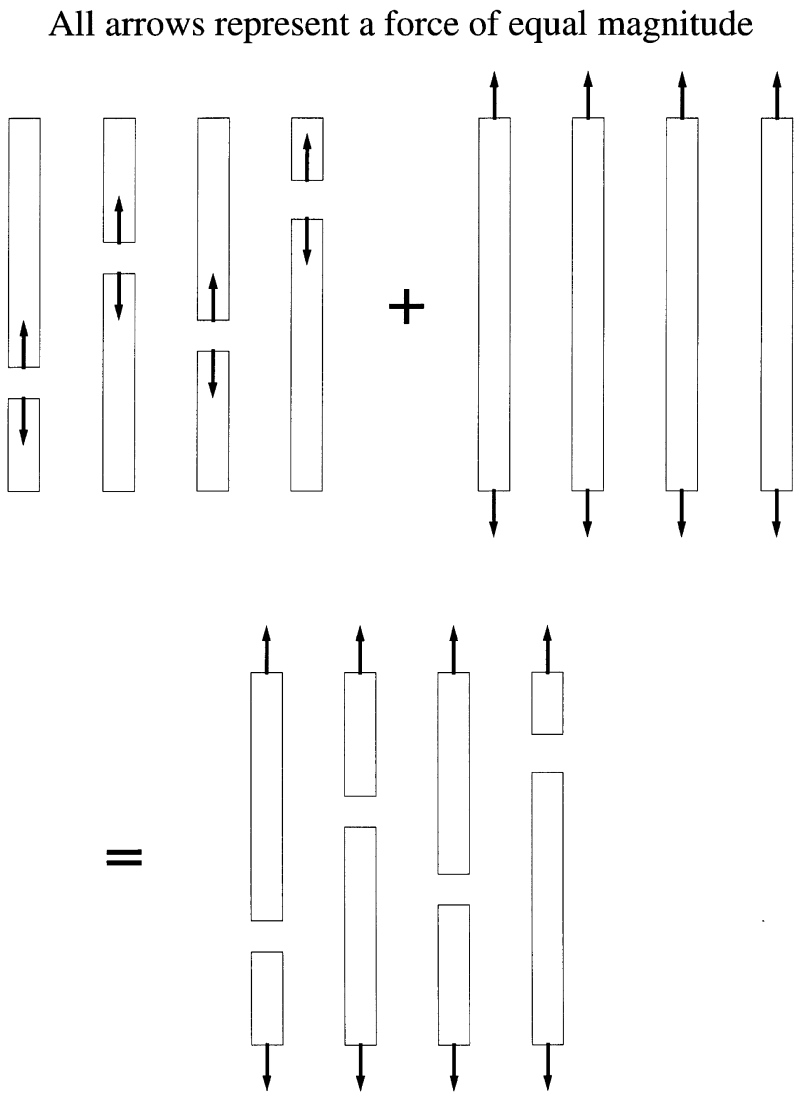

Fig. 2. A schematic of the superposition procedure used in the Break Influence Superposition technique.

Given that we can control the stress at any position in a fiber or matrix line of freedom using BIS, it is possible to model sliding using this method. Recall eqn (10a) which states that the normalized axial stress in a broken fiber in the sliding region increases linearly from the break. Therefore, we can model the sliding region as a continuous distribution of breaks with non-zero traction. The traction in this region before we superpose the uniform far field strain has the form

$$\frac{p_i(\xi)}{E_{\mathrm{f,m}}\varepsilon} = -1+\hat{\tau}_0|\xi-\xi_i| \tag{18}$$

where ξ_i is the position of the ith break. Then the set of equations given by eqn (16) becomes a set of integral equations governing the weight functions of the slip zones around the breaks,

$$\sum_{j=1}^{M}\left\{\int_{\xi_j}^{\xi_j+\hat{L}_{\mathrm{sR},j}} q_{ij}(\xi-\xi')w_{\mathrm{R}j}(\xi')\,\mathrm{d}\xi' + \int_{\xi_j-\hat{L}_{\mathrm{sL},j}}^{\xi_j} -\hat{L}_{\mathrm{sL},j}\,q_{ij}(\xi-\xi')w_{Lj}(\xi')\,\mathrm{d}\xi'\right\} = -1+\hat{\tau}_0|\xi-\xi_i| \tag{19}$$

where $\hat{L}_{\mathrm{sR},j}$ and $\hat{L}_{\mathrm{sL},j}$ are the normalized lengths of the sliding regions to the right and left of break j assuming the ξ direction increases to the right, and $w_{\mathrm{R}j}$ and $w_{\mathrm{L}j}$ are the weight functions for the right and left sliding regions for break j. Equation (19) ($i = 1$ to M) represents a set of Fredholm integral equations of the first kind governing the weight functions $w_{\mathrm{R,L}j}(\xi)$. The difficulty with this set of equations is that the lengths of the sliding zones are not known a priori. The final solution must be found by iteration given the boundary conditions that the magnitude of the shear stress just outside of a sliding region must be equal to the debond shear strength, $\hat{\tau}_{\mathrm{D}}$.

At this point the formulation is still a bit abstract so we will give two examples. First we will show the governing equation for the single fiber shear lag model with a single break, then we will solve the equations for a single fiber break on fiber $m = 0$, $n = 0$ in an infinite composite with no axial matrix stiffness and fibers arranged in a square array. For simplicity we will assume that the debond shear strength is equal to the shear sliding strength. Since we are dealing with a single break the slip zones must be symmetric, i.e. $\hat{L}_{\mathrm{sR}} = \hat{L}_{\mathrm{sL}} = \hat{L}_{\mathrm{s}}$. Equation (19) now reduces to one equation governing a single weight function. For the single fiber shear lag model the influence function appears in eqn (7), $q(\xi) = -\exp(-|\xi|)$. Therefore, the equation governing the weight function in the sliding region is

$$\int_0^{\hat{L}_{\mathrm{s}}}[-\exp(-|\xi-\xi'|)-\exp(-|\xi+\xi'|)]w(\xi')\,\mathrm{d}\xi = -1+\hat{\tau}_0\xi \tag{20}$$

The shear stress at the end of the sliding zone at $\xi = \hat{L}_{\mathrm{s}}$ is

$$\hat{\tau}(\hat{L}_{\mathrm{s}}) = \int_0^{\hat{L}_{\mathrm{s}}}[-\exp(-|\hat{L}_{\mathrm{s}}-\xi'|)-\exp(-|\hat{L}_{\mathrm{s}}-\xi'|)]w(\xi')\,\mathrm{d}\xi' = -\hat{\tau}_{\mathrm{D}} \tag{21}$$

No significance should be placed on the fact that the kernel function in eqn (21) is identical to the kernel function in eqn (20). The kernel for eqn (21) comes from eqn (8) for the shear stress on the fiber near the break. An exact solution exists for the weight function $w(\xi)$ in eqns (20) and (21). It is:

$$w(\xi) = \hat{\tau}_0\delta(\xi)+(\hat{\tau}_{\mathrm{D}}-\hat{\tau}_0)\delta(\xi-\hat{L}_{\mathrm{s}})+\frac{1}{2}(1-\hat{\tau}_0\xi) \quad \text{with} \quad \hat{L}_{\mathrm{s}} = \frac{1}{\hat{\tau}_0}-\frac{\hat{\tau}_{\mathrm{D}}}{\hat{\tau}_0} \tag{22}$$

where $\delta(\xi)$ is the Dirac delta function such that $\int_a^b f(\xi)\delta(\xi-c)\,\mathrm{d}\xi$ is equal to $f(c)$ if $a < c < b$, $f(c)/2$ if $c = a$ or $c = b$ and 0 otherwise. The solution for the weight function yields the same results for

fiber stresses as eqn (13). The solution to eqns (20) and (21) was also done numerically with a Gaussian quadrature method as described by Press et al. (1992), and a bisection method was used to find the appropriate $\hat{L}_s$. We will mention here only that the numerical results agree perfectly (from a numerical standpoint) with the exact solution given in eqn (13) and that the singular delta functions do not cause any numerical difficulties.

We now turn our focus to the infinite system and the effect of sliding on stress concentrations in neighboring fibers. The governing equation for the weight function in the sliding zone is

$$\int_0^{\hat{L}_s} [q_{0,0}(\xi-\xi')+q_{0,0}(\xi+\xi')]w(\xi')\,\mathrm{d}\xi' = -1+\hat{\tau}_0\xi \tag{23}$$

where $q_{0,0}$ is the influence function defined in eqns (5) and (6). For our study we assume that the debond shear strength is equal to the shear sliding stress. The definition of ξ is given in eqn (4). The normalization for the shear stress is

$$\hat{\tau} = -\frac{\mathrm{d}^2u}{\mathrm{d}\xi^2} = 4\sqrt{\frac{3\pi}{4}}\sqrt{\frac{E_f}{G_m}}\frac{\tau}{E_f\varepsilon} \tag{24}$$

This normalization is also valid for the shear sliding strength. The stress on a fiber located at position m, n is

$$\frac{\sigma_{m,n}(\xi)}{E_f\varepsilon} = 1+\int_0^{\hat{L}_s} [q_{m,n}(\xi-\xi')+q_{m,n}(\xi+\xi')]w(\xi')\,\mathrm{d}\xi' \tag{25}$$

where $q_{m,n}$ is given in eqns (5) and (6). The shear stress at the end of the sliding zone is

$$\hat{\tau}_{0,0}(\hat{L}_s) = \int_0^{\hat{L}_s} [t_{0,0}(\hat{L}_s-\xi')+t_{0,0}(\hat{L}_s+\xi')]w(\xi')\,\mathrm{d}\xi' = -\hat{\tau}_0 \tag{26}$$

where

$$t_{m,n}(\xi) = \frac{-\operatorname{sgn}(\xi)\displaystyle\int_0^{\pi}\int_0^{\pi}\cos n\theta\cos m\phi(\alpha^2\exp[-\alpha|\xi|])\mathrm{d}\theta\mathrm{d}\phi}{\displaystyle\int_0^{\pi}\int_0^{\pi}\alpha\mathrm{d}\theta\mathrm{d}\phi} \tag{27}$$

where α is given in eqn (5). Note that the sgn function and the absolute value arise due to the fact that the $t_{m,n}(\xi)$ are antisymmetric about $\xi = 0$ such that $t_{m,n}(-\xi) = -t_{m,n}(\xi)$. The solution to eqn (23) is obtained by a Gaussian quadrature method described by Press et al. (1992), and $\hat{L}_s$ is found using a bisection method.

Figures 3 and 4 show results for the axial stress in the broken fiber and the axial stress in the nearest neighbor fiber respectively. Beyerlein and Phoenix (1996) have formulated a model to handle sliding specifically for the two-dimensional (i.e. a single sheet of fibers and matrix) shear lag model of Hedgepeth (1961) and found similar trends to those found in Figs 3 and 4. There are multiple curves on each graph corresponding to different values of the parameter $1-\hat{\tau}_0/\hat{\tau}_{max}$ where

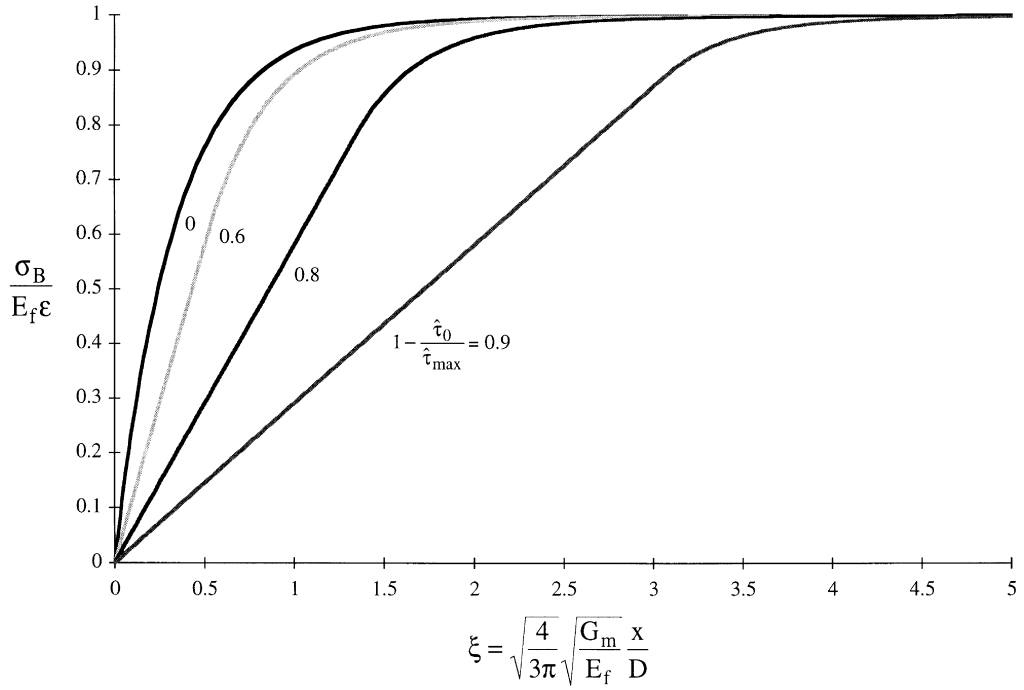

Fig. 3. The axial stress in a broken fiber as a function of ξ (the normalized distance from the break), for four values of the normalized shear sliding strength.

$\hat{\tau}_{max} = -t_{0,0}(\xi = 0)$ which in this case is 2.90 and represents the maximum normalized shear stress at the break. This parameter is also closely related to the ratio $\hat{L}_s/\hat{L}_{KT}$ where $\hat{L}_{KT}$ is the slip length in the Kelly and Tyson (1965) shear lag model that assumes that all of the stress recovery in the broken fiber is governed by sliding. The normalized lengths $\hat{L}_s$ and $\hat{L}_{KT}$ are

$$\hat{L}_s \approx \frac{1}{\hat{\tau}_0} - \frac{1}{\hat{\tau}_{max}}, \quad \hat{L}_{KT} = \frac{1}{\hat{\tau}_0} \tag{28a–b}$$

The right hand side of eqn (28a) is an upper bound on $\hat{L}_s$ and has a maximum error of about 2.7% where $1-\hat{\tau}_0/\hat{\tau}_{max} = 0.3$. Therefore $\hat{L}_s/\hat{L}_{KT} \approx 1-\hat{\tau}_0/\hat{\tau}_{max}$ high normalized shear sliding strength implies that the sliding length is much smaller than what is predicted by the simple Kelly and Tyson model, and low shear sliding stress creates sliding lengths that are comparable to the length predicted by the Kelly and Tyson model.

Figure 3 illustrates that as $\hat{\tau}_0$ approaches zero the axial stress distribution in the broken fibers approaches the bilinear profile predicted by the Kelly and Tyson model. Figure 4 shows that when $\hat{\tau}_0 \geqslant \hat{\tau}_{max}$ the stress concentration factor in the nearest neighbor fiber reaches its maximum value of 1.081. In this regime the system is no different from a well bonded system. As $\hat{\tau}_0$ decreases, the stress concentration factor in the nearest neighbor fiber also decreases until the point were $\hat{\tau}_0 \to 0$ and the stress concentration goes to one (no increase in stress due to the break).

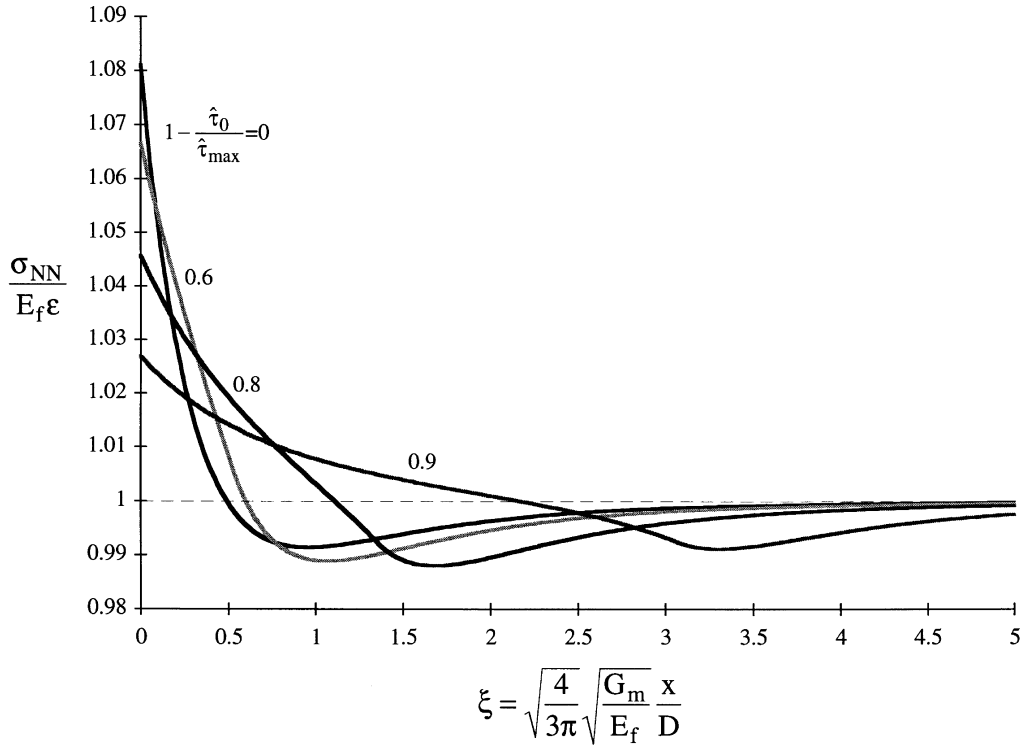

Fig. 4. The axial stress in a nearest neighbor fiber as a function of ξ (the normalized distance from the break), for four values of the normalized shear sliding strength.

Figure 5 is a plot of the maximum stress concentration in the nearest neighbor fiber as a function of $1-\hat{\tau}_0/\hat{\tau}_{max}$. Figure 6 is a plot of the inverse of the normalized distance from the break where the axial stress in the nearest neighbor fiber first falls to the far field applied stress (also called the positively affected length), $1/\hat{L}_1$, vs $1-\hat{\tau}_0/\hat{\tau}_{max}$. In general high stress concentrations are detrimental to composite strength, but when considering the statistical nature of fiber strength a more accurate statement would be that high stresses acting over long lengths of fiber are detrimental to composite strength. Notice in Figs 4–6 that as the stress concentration decreases the length of fiber that experiences an elevated stress increases.

It is of interest to consider whether the higher stress concentration acting over the shorter length when $\hat{\tau}_0$ is large is effectively worse for failing the material than the lower stress concentration acting over the longer length when $\hat{\tau}_0$ is small. We have developed one simple model to address this issue. Assume that we have applied load to a composite with no fiber breaks. In this situation all of the fibers have the same uniform stress and the same probability of failure. Now assume that a single fiber breaks and sliding is allowed at the interface. The axial stress in the broken fiber looks like a stress profile in Fig. 3 and the stress in a nearest neighbor fiber looks like the corresponding profile in Fig. 4. We can now calculate the probability that a nearest neighbor fiber

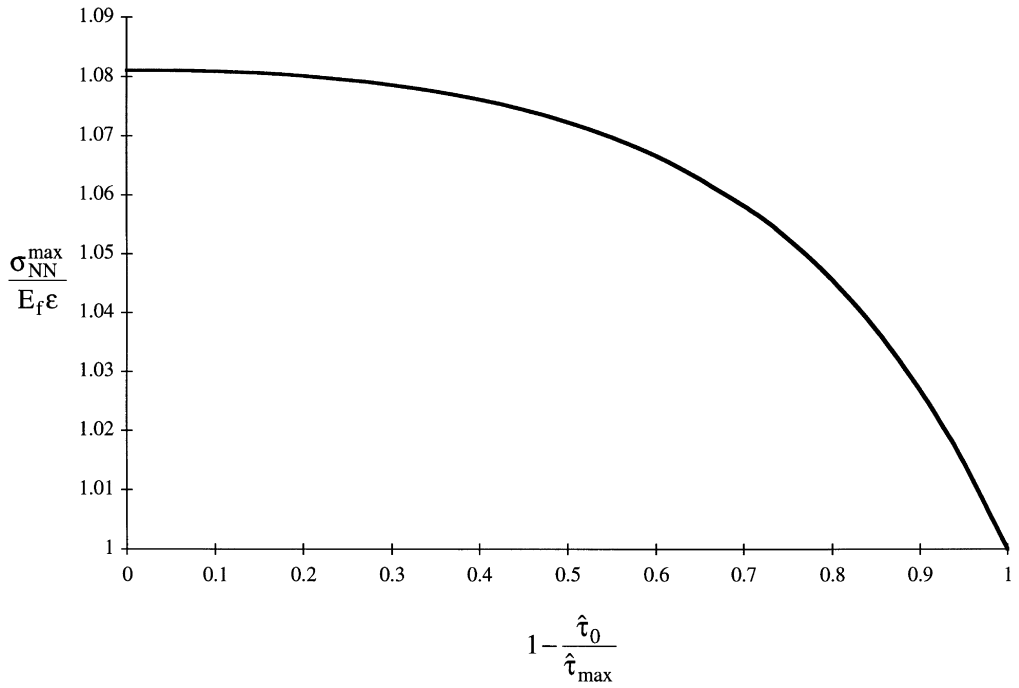

Fig. 5. The maximum stress concentration factor in a nearest neighbor fiber as a function of the normalized shear sliding strength.

will survive given that it was able to survive the initial stress required to break the failed fiber. Calculations of this type are fundamental to determining the probability of failure of a material experiencing non-uniform stresses, and have been done previously by many authors including Phoenix and Sexsmith (1972), Thouless and Evans (1988) and Schwietert and Steif (1990). The probability of survival for a fiber experiencing a varying axial stress distribution, $\sigma(x)$, given that it survived an initial uniform stress of $\sigma = E_f\varepsilon$, is

$$P_s = \frac{\exp\left[-\frac{2}{L_0}\int_0^{L_1}\left(\frac{\sigma(x)}{S_0}\right)^m \mathrm{d}x\right]}{\exp\left[-\frac{2L_1}{L_0}\left(\frac{E_f\varepsilon}{S_0}\right)^m\right]} \tag{29}$$

where $x = 0$ is the plane of the break. We have assumed that the failure statistics of the fibers is governed by a Weibull distribution. The parameters L_0 and S_0 are the Weibull strength and length parameters, m is the Weibull modulus and $-L_1$ and L_1 are the limits within which the fiber is able to fail. The relevant limit L_1 lies where the axial stress in the nearest neighbor fiber first falls to the initial applied stress as shown in Fig. 6. The probability of failure in the region of the fiber where the stress has decreased is zero. In general, eqn (29) can be represented in a simpler form as

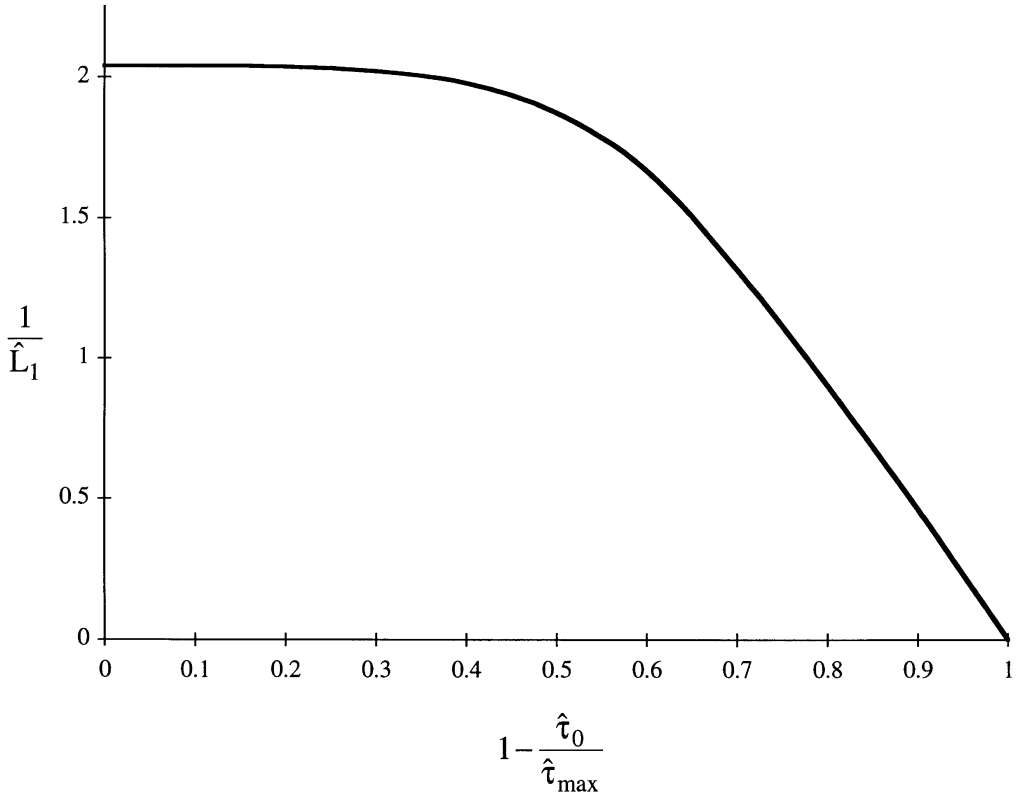

Fig. 6. The inverse of the length over which the axial stress in a nearest neighbor fiber is elevated above the far field applied stress as a function of the normalized shear sliding strength.

$$P_s = \exp\left[-2k\left(\frac{E_f\varepsilon}{S^*}\right)^m\right] \tag{30}$$

where

$$S^* = S_0\left[\sqrt{\frac{4}{3\pi}}\sqrt{\frac{G_m}{E_f}}\frac{L_0}{D}\right]^{1/m}$$

$$k = \int_0^{\hat{L}_1}\left[\frac{\sigma_{nn}(\xi)}{E_f\varepsilon}\right]^m d\xi - \hat{L}_1$$

$$\hat{L}_1 = \sqrt{\frac{4}{3\pi}}\sqrt{\frac{G_m}{E_f}}\frac{L_1}{D} \tag{31a–c}$$

Here S^* is a characteristic strength for the composite, $\sigma_{nn}(\xi)$ is the stress in the fiber that is a nearest neighbor to the break and k is a dimensionless parameter governing the probability of

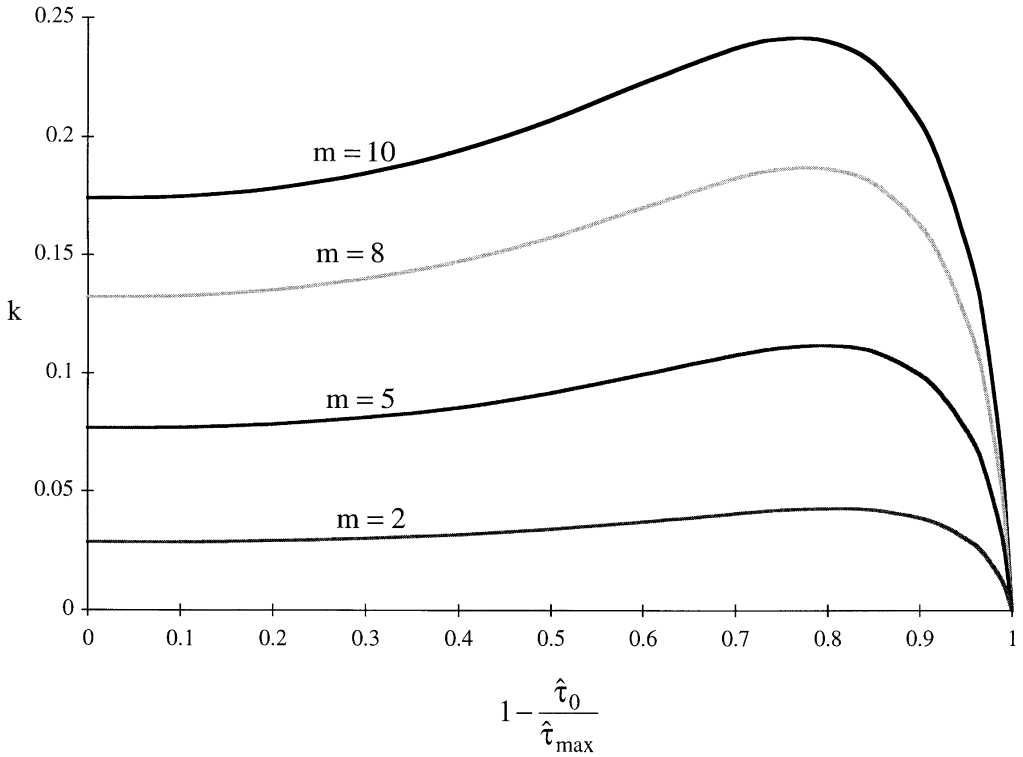

Fig. 7. A measure of the probability of failure, k, for a fiber neighboring the break as a function of the normalized shear sliding strength, for four values of the Weibull modulus.

failure of the fiber. Large values of k imply that the nearest neighbor fiber is likely to fail, while a k value of zero implies that the fiber will not fail and further load is needed to cause another break. The limit of $k = 0$ implies global load sharing. Since no closed form expression exists for the stress profile in a fiber neighboring a break in the slipping system, the value of k was determined by numerical integration of the results for the axial stress in the nearest neighbor fiber. Figure 7 is a plot of the value of k as a function of $1-\hat{\tau}_0/\hat{\tau}_{max}$. The plot shows that k is not monotonically decreasing with decreasing $\hat{\tau}_0$ and therefore lower stress concentrations do not necessarily imply lower probabilities of failure for the neighboring fibers. It can be seen that $k = 0$ (GLS) occurs only for $\hat{\tau}_0 = 0$.

A stress concentration factor of 1, i.e. no stress concentration in the neighboring fiber, occurs when the sliding length is equal to the sliding length predicted by Kelly and Tyson (1965). This implies that the axial stress profile in the broken fiber is bilinear. This situation, where there are no stress concentrations and the broken fiber has a bilinear stress recovery profile, are exactly the assumptions used in infinite fiber global load sharing models (Curtin, 1991; Hui et al., 1995). As noted above, this occurs when $\hat{\tau}_0 = 0$. The parameter $\hat{\tau}_0 = 0$ when the matrix is rigid in shear, τ_0 is zero, or the far field applied strain is infinite. Therefore, GLS occurs in composites when there is sliding at the fiber/matrix interface and the matrix has infinite shear modulus. The conditions

where GLS-like behavior should occur are when the matrix is relatively stiff, the interfacial sliding stress is low, and the fibers are relatively strong such that breaks occur only at high strains. The strength of GLS materials has been studied extensively by many authors. The most notable works are the approximate strength model formulated by Curtin (1991), the exact treatment of the single filament composite by Hui et al. (1995) and the investigation of size effects by Phoenix et al. (1997).

4. Numerical solution to shear lag models

To this point we have discussed only exact solution procedures for the governing shear lag equations. With the method that we have proposed to formulate the governing shear lag equations, it is very easy, and in some cases less tedious, to solve these equations using a numerical finite element method. In doing this we return to the model of Cox et al. (1994).

Equation (1) represents the set of differential equations that governs the displacements in the fibers of the shear lag model. These equations were derived using the finite element method. In other words, the system was discretized into a set of nodes with fiber and matrix elements connecting the nodes, a displacement field consistent with the nodal displacements was assumed in each element and then the principle of virtual work was utilized to determine the spring stiffnesses that represent the fibers and matrix. To obtain the final governing equations, the discretization length in the x-direction was taken to approach zero. The resulting infinite system of linear, ordinary differential equations lends itself to a solution by a Fourier transformation technique.

Utilization of the Fourier transformation method requires that the model system be relatively simple. Axial matrix stiffness, and uneven fiber spacing are complications that prohibit the use of the Fourier transformation technique. It is possible to solve for the eigenvalues and eigenvectors of the system but this procedure can be tedious. Instead, we will use the entirely numerical finite element matrix method as the solution procedure to investigate the effects on stress concentrations. The numerical calculations model the same system as described by eqn (14), but now the discretization length, Δx, is not infinitesimal. The fibers are still one-dimensional springs and the matrix is represented by brick elements with degrees of freedom in the x-direction. For all of the numerical finite element results presented in the next sections, the array is 13×13 fibers in the z- and y-directions, and the number of elements along the length of a fiber is 80. The total length of the fibers is chosen such that the stress in the broken fiber has recovered to at least 99% of the far field applied stress. Each calculation takes between 1 and 5 min on a Silicon Graphics Indigo workstation.

For the purposes of comparing the numerical finite element calculation to the results for the infinite array given by the influence function in eqns (3)–(6), the first results to be discussed will be for the well bonded case. Figure 8 is a two-dimensional representation of the three-dimensional model. For the case of a single break, three mutually perpendicular symmetry planes exist with a common point at the break. This allows us to consider one eighth of the entire three-dimensional system. Fibers lying on a symmetry plane are given half of the stiffness of a full fiber and the broken fiber is given one quarter of the stiffness of an entire fiber. Figure 8 illustrates that all of the nodes on the plane of the break are given zero displacement except for the broken fiber which is required to have zero nodal force. All of the nodes on the boundary opposite to the plane of the break are given a uniform displacement that is related to a uniform applied strain. Figures 9 and

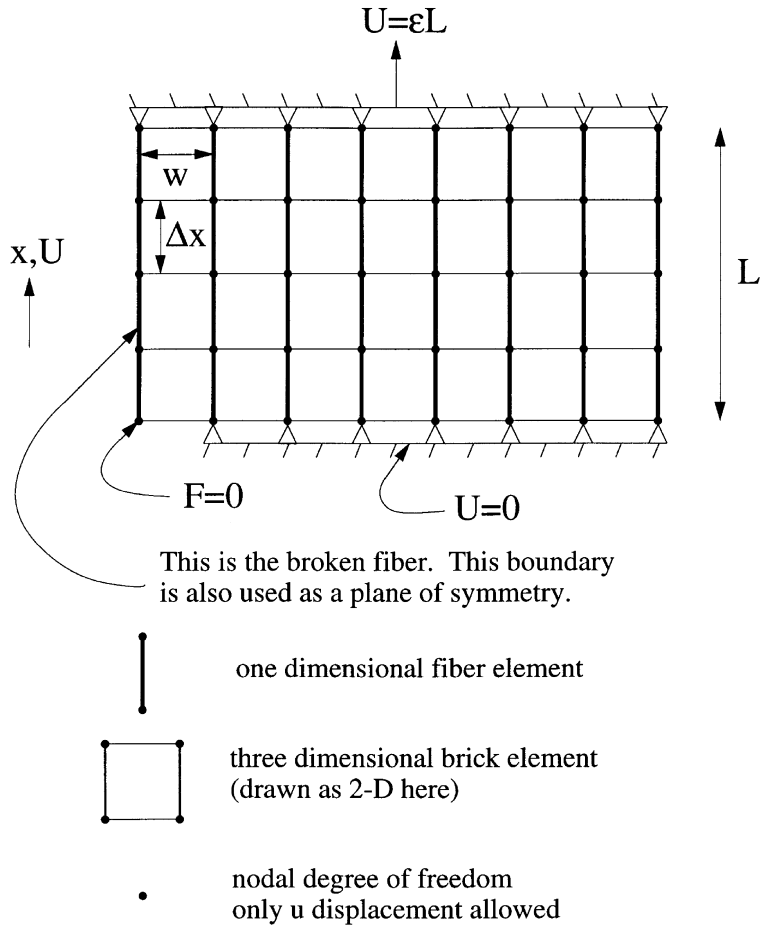

Fig. 8. A 2D representation of the model when the finite element matrix method is used as the solution procedure. Boundary conditions are only needed on the top and bottom surfaces because the nodes are only allowed to displace in the x-direction. If the matrix has axial stiffness then a second step is required to enforce the condition of zero axial stress at the break.

10 are plots of the axial stress in the broken and in a nearest neighbor fiber as a function of the distance from the break plane in non-dimensional units ξ. The circles are the numerical finite element results and the crosses are the results from eqns (3)–(6). These plots demonstrate that it is adequate to use a finite 13×13 array of fibers, and a finite model length with 80 elements along a fiber, to represent the stresses present near a single fiber break in a large composite. The results for the stresses in the broken fiber and the nearest neighbor fibers are fitted very well to the following functions:

$$\frac{\sigma_{\mathrm{B}}(\mathrm{x})}{E_{\mathrm{f}}\varepsilon} = 1 - \exp\left(-1.86\sqrt{\frac{G_{\mathrm{m}}}{E_{\mathrm{f}}}}\frac{x}{D}\right) \tag{32}$$

and

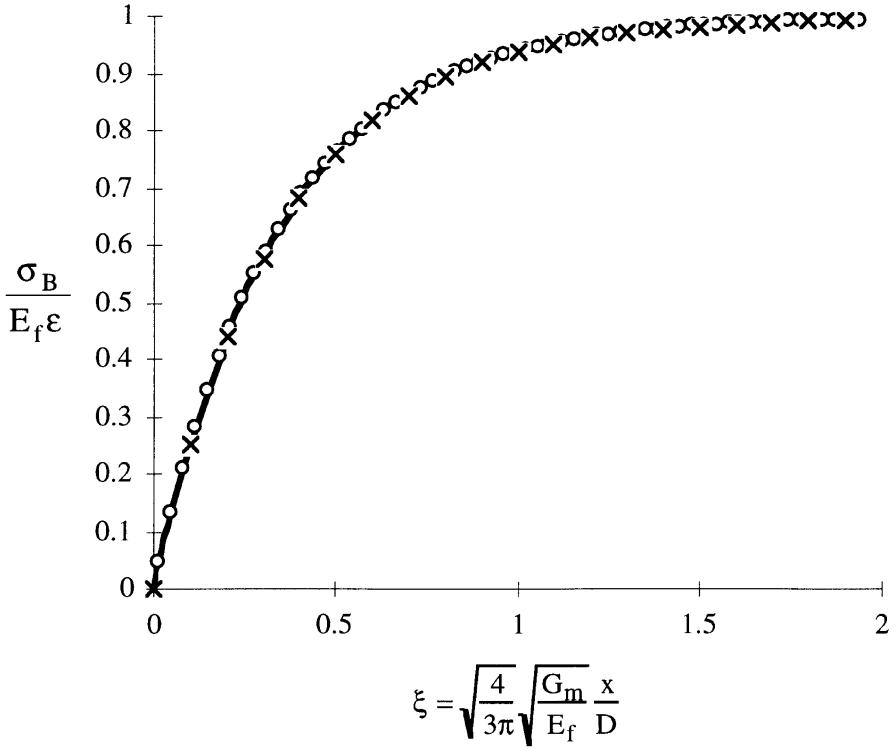

Fig. 9. The axial stress in a broken fiber as a function of the non-dimensional length ξ. The fibers are well bonded to the matrix, the matrix has no axial stiffness, and the fibers are arranged in a perfect square array. x is the influence function solution for the infinite array of fibers, the circles are the finite element results, and the solid line is the fit of eqn (32).

$$\frac{\sigma_{\mathrm{NN}}(\mathrm{x})}{E_{\mathrm{f}}\varepsilon} = 1 - \exp\left(-1.47\sqrt{\frac{G_{\mathrm{m}}}{E_{\mathrm{f}}}}\frac{x}{D}\right) + 1.081\exp\left(-1.57\sqrt{\frac{G_{\mathrm{m}}}{E_{\mathrm{f}}}}\frac{x}{D}\right) \tag{33}$$

where σ_{B} is the axial stress in the broken fiber and σ_{NN} is the axial stress in the nearest neighbor fiber. These functions are shown as solid lines in Figs 9 and 10. The functional form for the stress in the broken fiber follows from the original shear lag model formulated by Cox (1952). The value of 1.86 in the exponential is used to fit the numerical results and is not present in the original Cox paper. We emphasize that these functions are not exact solutions from the influence function but rather closed form fits to the exact solution.

The finite element model presented here is essentially identical to the model presented in eqns (1)–(6). It solves the same governing equations developed by Landis et al. (1998). Equations (3)–(6) are the exact solution to the set of equations given by eqn (1). The final result requires a numerical integration which can give the desired result to almost any precision necessary. On the other hand, the finite element results are a completely numerical solution to the equations. The system is broken up into discrete nodal degrees of freedom, a set of linear matrix equations is

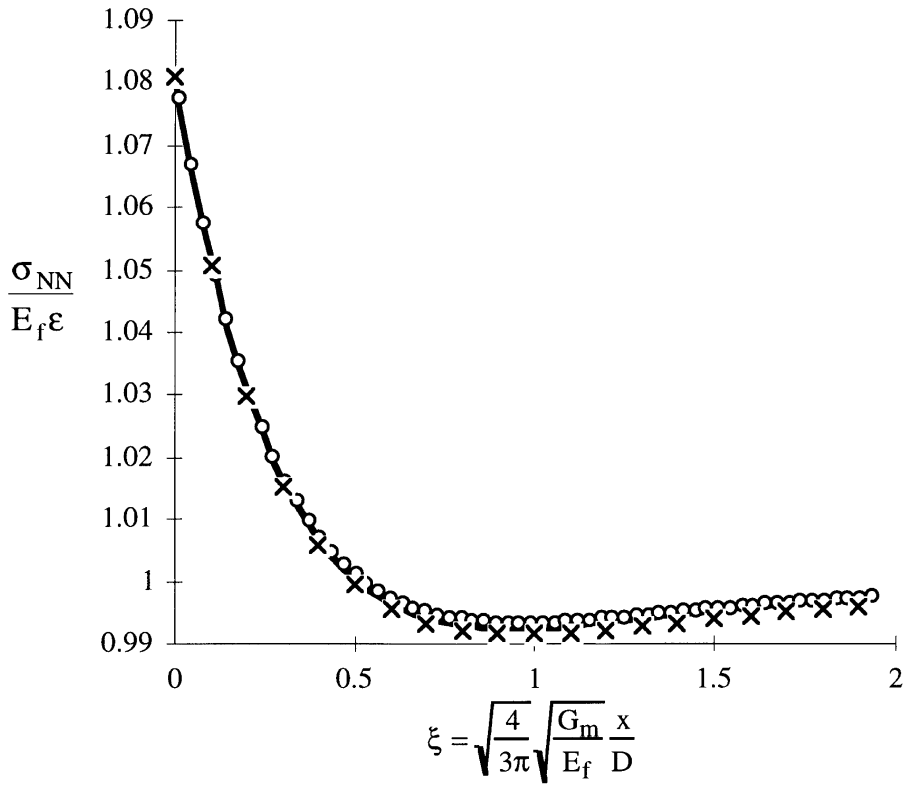

Fig. 10. The axial stress in a nearest neighbor fiber as a function of the non-dimensional length ξ. The fibers are well bonded to the matrix, the matrix has no axial stiffness, and the fibers are arranged in a perfect square array. x is the influence function solution for the infinite array of fibers, the circles are the finite element results, and the solid line is the fit of eqn (33).

obtained, the matrix is inverted and the final solution is calculated. It is no longer possible to deal with an infinite array of fibers and the final results are subject to the same discretization errors that all numerical models suffer from. The models to be presented in the next sections use the numerical finite element method as the solution procedure. All of these models are shear lag models.

5. Well bonded fibers in a matrix with axial stiffness

To this point we have only considered matrices that cannot carry any axial loads. This assumption is most valid for matrices that are cracked or possibly yielded due to tensile stresses that existed in the composite prior to any fiber breaks. For matrices with high strains to failure and relatively high stiffness, the assumption that $E_m = 0$ is no longer valid. Recent experimental work, Wagner et al. (1996), has demonstrated the fact that stress concentrations in composites with

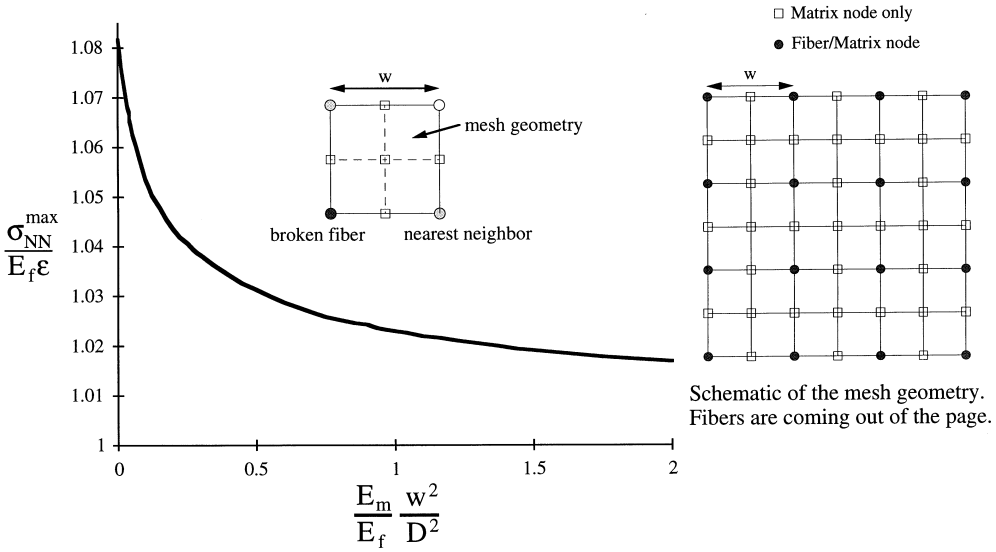

Fig. 11. The maximum stress concentration in a nearest neighbor fiber as a function of the axial matrix stiffness. The stress concentration factor in a nearest neighbor fiber decreases as the axial stiffness of the matrix increases. The extra matrix nodes allow the crack to be isolated to the fiber.

tough matrices do depend on the axial stiffness of the matrix. All of the shear lag models that do not consider the axial stiffness of the matrix material are not able to predict this behavior.

To model axial matrix stiffness and to maintain the spirit of simplicity of shear lag modeling, extra degrees of freedom must be placed among the fibers and this arrangement is shown in Fig. 11. Since the axial stiffness of the matrix depends on both the Young's modulus of the matrix, E_m, and the area, w^2, of the matrix between the fibers, the dimensionless parameter $E_m w^2/E_f D^2$ is used to characterize the amount of matrix stiffness in the system. No sliding is allowed to occur at the interface, so the calculation is linear elastic. Due to the introduction of extra nodes in the matrix the solution of the problem does not lend itself to the Fourier transformation solution method. Therefore, we use a numerical finite element procedure to obtain the results. The model is a uniformly spaced, 13×13 array of fibers with extra matrix nodes in the pattern shown in Fig. 11. There are 80 elements of length Δx along every fiber. As in the previous models, the stiffness of the 'springs' that represent the matrix are determined by the finite element method. The stiffness terms for an element are given in Appendix A. There are degrees of freedom lying entirely within the matrix which are used to introduce the effect of having intact matrix material surrounding the broken fiber. The procedure for solving the problem of a uniformly strained composite with a single stress free fiber break requires two steps. The first step has been described in the previous section and is illustrated in Fig. 8. After this step is completed and if the matrix has axial stiffness, as it does in this case, then the stress at the tip of the broken fiber will be compressive. In order to enforce the condition of zero stress at the break, we must now superpose on this solution the solution for a uniform strain. The uniform strain is tensile and its magnitude is such that it will negate the compressive stress at the fiber break from the initial solution. The stress at any position in the model is the stress from the first solution plus the stress from the uniform strain solution.

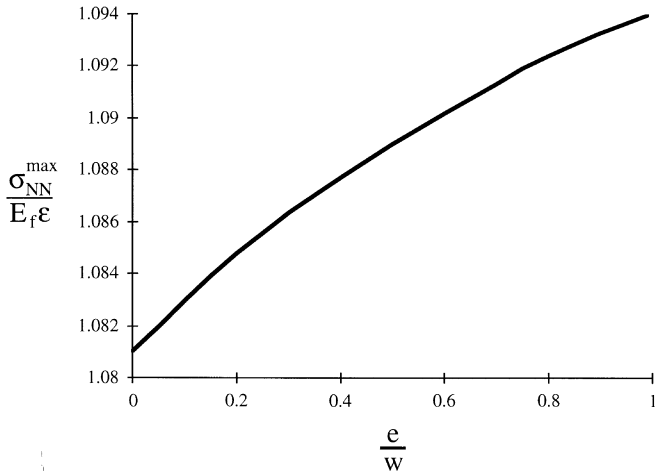

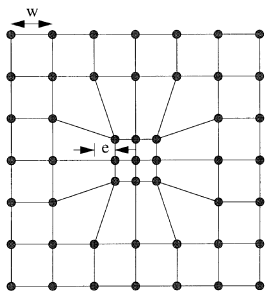

Schematic of the mesh geometry.
The fibers are coming out of the page.
The central fiber is broken.

Fig. 12. The stress concentration factor in a nearest neighbor fiber with all of the immediate neighbors having close spacing as a function of the relative perturbation size.

Figure 11 is a plot of the maximum stress concentration in a nearest neighbor fiber for a given value of the matrix stiffness. When the matrix has zero stiffness the stress concentration in the nearest neighbor is 1.081 as expected. As the relative stiffness of the matrix $E_m w^2/E_f D^2$ increases, the maximum stress in the nearest neighbor fiber decreases as shown in Fig. 11. Shear lag models that neglect axial matrix stiffness cannot predict the effects of increasing the matrix Young's modulus or fiber spacing on stress concentrations. We have presented a mechanically consistent method for determining these effects.

6. Uneven fiber spacing

As mentioned earlier, it is difficult to process composites so that the fibers form a perfectly uniform array. Also, experimental measurements, Wagner et al. (1996), are most often done on composites with non-uniform fiber spacing. Almost all attempts at modeling composites, including the models discussed previously in this paper, assume that the fibers are arranged in a periodic array, be it square, hexagonal or something else. In this section we will address what happens to stress concentrations around breaks when there is some type of eccentricity in the placement of fibers near a break. Examples of the meshes that were used are shown in Figs 12 and 13. We assume that the fibers are perfectly straight and parallel coming out of the plane of the schematics. Also, the fibers are well bonded to the matrix which has zero axial stiffness. Again this type of fiber configuration does not lend itself to the Fourier transformation solution method. The numerical finite element method is used. All of the elements that are square have stiffnesses as given in Appendix A, while elements near the displaced fiber(s) that are not square in their plan have stiffnesses that are determined by the isoparametric finite element formulation, Irons (1966). Once the stiffness matrix is assembled the calculation is linear elastic. The boundary conditions are

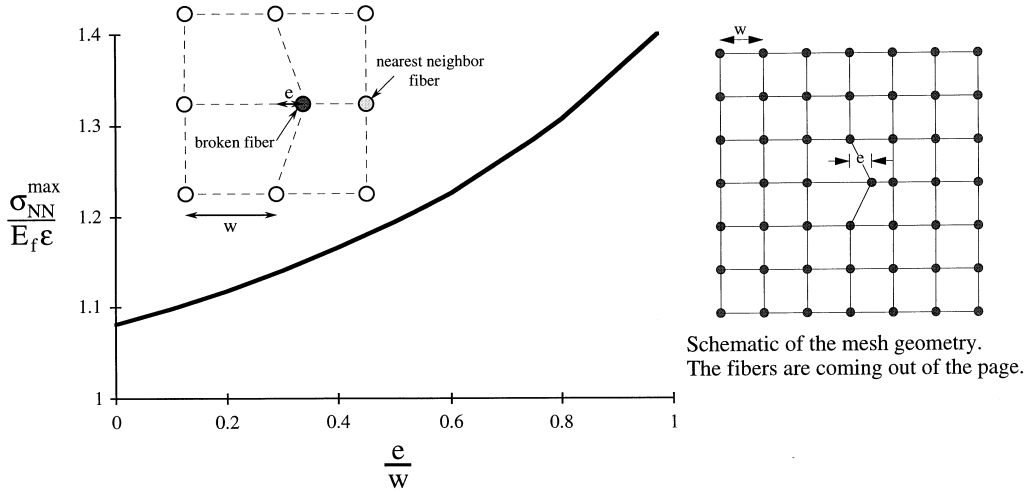

Fig. 13. The stress concentration factor in the nearest neighbor fiber with the broken fiber perturbed from its central position as a function of the relative perturbation size.

applied as shown in Fig. 8 and as discussed in previous sections. Notice that the mesh in Fig. 13 has only one of the two transverse planes of symmetry and therefore one quarter of the entire model enters into the solution instead of only one eighth.

Two types of fiber spacing eccentricity are considered. The first type of eccentricity is where all of the eight fibers surrounding the break are moved toward the broken fiber such that the new spacing between these fibers is reduced by the distance e, as shown in Fig. 12. The second type of eccentricity moves only the broken fiber by a distance e toward one of the nearest neighbor fibers, as shown in Fig. 13. All of the other fibers in the 13×13 array are in their proper positions and the only perturbation in the spacing is near the fiber break.

First let us consider the case where all immediately neighboring fibers are moved closer to the broken fiber. Figure 12 is a plot of the maximum stress in a nearest neighbor fiber as a function of the eccentricity ratio e/w, where w is the unperturbed fiber spacing. As shown in the graph, a maximum value of 1.094 for the stress concentration factor in a nearest neighbor fiber is obtained. Since there are eight neighboring fibers, an upper bound on the stress concentration factor must be 1.125 (if other fibers on this plane do not have a SCF less than 1). In this situation all of the neighboring fibers would share the load shed by the broken fibers equally and no other fibers in the array would be affected by the break. We have seen from other models that all fibers at a finite distance from the break can 'feel' the presence of the break. Any stress perturbation in a fiber neighboring a break must certainly perturb the stress state in a fiber neighboring it further from the break. Therefore, it should be impossible to reach a value for the stress concentration of 1.125. This fact is illustrated in Fig. 12.

Next consider the case were the broken fiber is moved toward one of the neighboring fibers by a distance e. Figure 13 is a graph of the nearest neighbor stress concentration as a function of e/w. A maximum stress concentration of 1.41 is approached as the eccentricity ratio approaches 1.

Following the same reasoning as in the previous paragraph, the upper bound on the stress concentration factor in the nearest neighbor must be 2. However, due to the long range load sharing that is present in this model, this bound is not reached.

These perturbations in the fiber arrangement can be interpreted as local increases in volume fraction. The results show that the two perturbations considered here give dramatically different results. A more uniform change in the local spacing gives rise to only a slight increase in the stress concentration on a neighboring fiber, while a very localized relocation of one fiber yields a significant increase in the stress concentration.

7. Discussion

We have attempted to characterize the stress concentrations that occur in fibrous composite materials. The finite element method was used to generalize an idealized shear lag model of Landis et al. (1998). The 'perfect' composite model assumes that the fibers are well bonded to the matrix, the matrix has zero axial stiffness and the fibers are arranged in a perfect square array. A new formulation to represent sliding in any shear lag system was presented and used to investigate the effects of sliding on fiber stress concentrations. A finite element model was used to relax the zero matrix axial stiffness and uniform fiber spacing assumptions and to investigate the effects on the stress concentrations near a single broken fiber. For the case of the 'perfect' composite the numerical finite element model was shown to be in excellent agreement with the exact solution of the influence function model.

The most important result from the 'perfect' composite model is not the magnitude of the stress concentration, but rather the characteristic length over which the stresses are elevated above the far field applied stress. The solution of the model leads to the normalization of lengths,

$$\xi = \sqrt{\frac{4}{3\pi}}\sqrt{\frac{G_{\mathrm{m}}}{E_{\mathrm{f}}}}\,\frac{x}{D}.$$

The term $\sqrt{G_{\mathrm{m}}/E_{\mathrm{f}}}$ in the normalization allows us to easily relate one fiber/matrix system to another and indicates that the main effect of changing the moduli ratio is to rescale the lengths over which stress elevation takes place in fibers adjacent to broken ones. This normalization carries over into the other models that relax the 'perfect' assumptions. The reason it is important to consider the lengths over which stress concentrations act and not just the stress concentration magnitude is that fibers do not have a deterministic strength. Instead, flaws are distributed statistically along the length of the fiber. Each of these flaws has a strength associated with it. Therefore, in order to fail a fiber the stress at a specific flaw site must be higher than that flaw's strength. If the stress is elevated along a fiber over a long distance, then more flaws will experience the high stress, and the probability that a weak flaw will be sampled is greater.

A second interesting behavior of the 'perfect' composite system is that the magnitude of the stress concentration does not depend on the fiber to matrix moduli ratio. This arises due to the assumptions that the matrix has no axial stiffness and only axial (x) displacements are allowed. Another consequence of the zero axial matrix stiffness shear lag model is that the fiber spacing does not affect the magnitude or the length over which the stress concentrations act. This can be

explained by examining the assumed geometry of the matrix. Between any four neighboring fibers the matrix is assumed to be square. Since the fibers are assumed to be one-dimensional, the matrix does not have holes where the fibers are located. Consider a square piece of material loaded in the same out of plane fashion that a matrix element would be loaded. The shearing stiffness (load to displacement ratio) of this structure is independent of the actual size of the square. Therefore, the spacing between fibers does not enter the formulation of the shear lag model when the matrix is assumed to have no axial stiffness. In reality the matrix does have holes where the fibers are positioned. As the spacing between fibers is decreased the effects of the holes becomes more pronounced because the relative size of the holes increases. To fully investigate the effects of fiber spacing, and thus volume fraction, other methods such as three-dimensional finite element calculations are required.

The first imperfection that was investigated in this work was the case where the broken fiber is able to debond from the matrix and slide with a constant shear stress acting at the interface. This type of behavior is generally desirable because it is a nonlinear process that tends to reduce stress concentrations in the composite and increases the fracture toughness. The magnitude of the stress concentration was shown to depend on $\hat{\tau}_0$ which is equal to $\sqrt[4]{3\pi/4}\sqrt{(E_f/G_m)(\hat{\tau}_0/E_f\varepsilon)}$. The maximum stress concentration factor in the nearest neighbor fiber and the length over which the axial stress is elevated above the far field applied stress were plotted against $1-\hat{\tau}_0/\hat{\tau}_{max}$.

Consider a fiber that is broken before any strain is applied to the composite. As load is first applied to the composite, the bond between the fiber and matrix will remain intact. The system is well bonded and the stress concentration in the neighboring fiber will be 1.081. The stress concentration factor will remain at 1.081 until enough strain is applied to cause the shear stress near the tip of the broken fiber over a significant area of the interface to reach τ_0, the critical shear sliding stress. Upon further loading the slip length will increase, and the stress concentration in the nearest neighbor fibers will drop according to Fig. 5.

What does this mean in terms of global or local load sharing? High stress concentrations occur at low applied strains when fiber failure is least likely to occur, and low stress concentrations occur at high applied strains when fiber failure is extensive. In order to answer this question more detailed calculations would have to be performed that include the statistics of fiber failure and allow for multiple breaks to interact. These types of calculations are beyond the scope of this paper. A few qualitative statements can be made about global versus local load sharing. First, a low critical shear sliding stress will cause composite behavior to be closer to the GLS regime. This is due to low values of τ_0 causing relatively long slip lengths. Second, a high matrix shear modulus will induce GLS-type behavior. The higher the matrix shear modulus, the closer the normalized shear sliding strength is to zero, and the smaller the stress concentrations. Finally, composites with stronger fibers will also approach the GLS regime. Strong fibers require high strains to cause failure, and the normalization of $\hat{\tau}_0$ implies that high strains reduce the relative shear sliding resistance, bring about relatively long slip zones, and consequently cause stress concentrations to be low. Generally, any characteristics that cause slip zones to be long and stress concentrations to be low imply a tendency towards global load sharing.

After the effects of sliding were investigated, the assumption that the matrix has no axial stiffness was relaxed. The finite element method gives a straightforward procedure for adding axial stiffness to the matrix in a mechanically consistent manner. Interpreting the results of the shear lag models with axial matrix stiffness is not as simple as the implementation. In order to keep shear lag models

as simple and useful as possible, it is necessary to use a small number of degrees of freedom. When this is done, the exact location of the crack tip at a fiber break becomes blurred. When there is zero axial stiffness in the matrix, this question is irrelevant because the fibers must carry all of the applied load anyway. However, when the matrix is able to carry load as well, careful modeling and some interpretation is needed.

The model we introduced added extra degrees of freedom in the matrix in order to effectively isolate the crack in the fiber. This model is relevant to systems where the fibers are well bonded to the matrix, but the matrix has sufficient toughness such that cracks that initiate in fibers do not propagate into the matrix. When this type of behavior occurs, the stress concentration factor in a nearest neighbor fiber diminishes as the axial stiffness of the matrix increases. Shear lag models that ignore axial matrix stiffness simply cannot predict these effects. The axial stiffness of the matrix consists of two parts, the Young's modulus of the matrix, E_m, and the area of the matrix, w^2. The axial stiffness per unit length of the matrix is then $E_m w^2$. The w^2 term can have two different simple interpretations. One approach would be to let w be the center to center fiber spacing. This is reasonable, based on the geometry of the system. The second interpretation would be to let w^2 be equal to the actual area between four fibers, accounting for the holes that the fibers leave in the matrix. This is a reasonable assumption because the Young's modulus of the shear lag composite, E_c, would then be given by the rule of mixtures, $E_c = fE_f + (1-f)E_m$, where f is the volume fraction of fibers being modeled. Again, this problem with the interpretation does not arise when $E_m = 0$ because the fiber spacing does not enter into the solution.

The final 'imperfection' that was considered was uneven fiber spacing. Two special cases of fiber spacing eccentricity were modeled. It was shown that a relatively uniform change in local fiber spacing (fiber volume fraction) causes less severe stress concentrations than when a single fiber is placed closer to a broken fiber. The possibility arises that an arrangement of fibers could occur randomly that is relatively weak, i.e. the stress concentrations in the cluster are higher than usual because of fluctuations in fiber spacing. This would be expected to be an initiation site for a fiber failure. Whether this failure would grow into the macroscopic defect which fails the composite would depend on the strengths of the surrounding fibers.

In the past, the matrix material in three dimensional shear lag models was represented by springs in an arbitrary fashion. The models presented in this paper still represent the matrix by springs, but the stiffnesses of these springs are determined in a mechanically consistent fashion by the finite element method. With the exception of some two-dimensional models, shear lag modeling has been limited to the assumptions that fibers are well bonded to the matrix, the matrix has zero axial stiffness and the fibers are arranged in a perfect array. The utility of these assumptions is that the model can almost be solved in closed form, requiring only a numerical integration to obtain the final solution. The problem with the model is that real composites never satisfy these assumptions.

The finite element method used here allows for a straightforward approach to model the effects of fiber/matrix interface sliding, axial matrix stiffness and uneven fiber spacing. This paper discusses each of these effects separately, but the model is not limited to the calculations presented here. Any combination of the above factors can be included. This is especially useful for comparison to experimental measurements where the control of fiber placement is not precise.

The stress concentration factor on a nearest neighbor fiber to a single broken fiber in a perfect square array, where the fibers are bonded to the matrix, and the matrix does not carry any axial loads is 1.081. Sliding at the fiber/matrix interface is a nonlinear process similar to plasticity that

reduces and spreads out the stress concentrations in the neighboring fibers. If the crack in the broken fiber does not extend significantly into the surrounding matrix, the addition of matrix stiffness lowers the stress concentrations in neighboring fibers. When fibers are perturbed from their regular positions the stress concentration increases as the neighboring fiber moves closer to the broken fiber. The quantitative effects of these factors on the strength of composites is beyond the scope of this paper, but qualitatively, lower stress concentrations along with smaller lengths that these stresses act on lead to higher composite strength.

Acknowledgements

The work was sponsored by the Advanced Research Projects Agency through the University Research Initiative at the University of California, Santa Barbara (ONR Contract N-0014-92-J-1808).

Appendix A

The stiffnesses of a matrix element with the node numbering shown below are

$$K_{11} = K_{22} = K_{33} = K_{44} = K_{55} = K_{66} = K_{77} = K_{88} = \frac{2}{9}G_{\mathrm{m}}\Delta x + \frac{1}{9}E_{\mathrm{m}}\frac{w^2}{\Delta x}$$

$$K_{12} = K_{34} = K_{56} = K_{78} = K_{15} = K_{26} = K_{37} = K_{48} = -\frac{1}{18}G_{\mathrm{m}}\Delta x + \frac{1}{18}E_{\mathrm{m}}\frac{w^2}{\Delta x}$$

$$K_{13} = K_{18} = K_{27} = K_{24} = K_{36} = K_{45} = K_{57} = K_{68} = -\frac{1}{36}G_{\mathrm{m}}\Delta x - \frac{1}{18}E_{\mathrm{m}}\frac{w^2}{\Delta x}$$

$$K_{14} = K_{23} = K_{58} = K_{67} = \frac{1}{9}G_{\mathrm{m}}\Delta x - \frac{1}{9}E_{\mathrm{m}}\frac{w^2}{\Delta x}$$

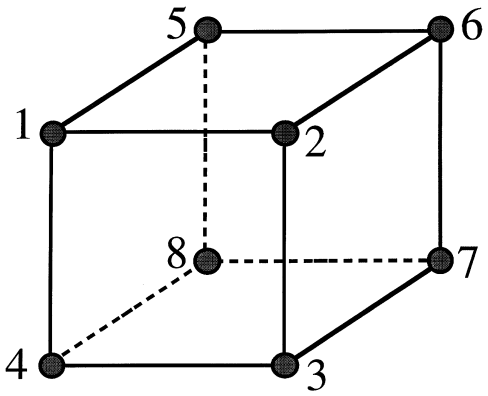

$$K_{16} = K_{25} = K_{38} = K_{47} = -\frac{1}{9}G_{\mathrm{m}}\Delta x + \frac{1}{36}E_{\mathrm{m}}\frac{w^2}{\Delta x}$$

$$K_{17} = K_{28} = K_{35} = K_{46} = -\frac{1}{18}G_{\mathrm{m}}\Delta x - \frac{1}{36}E_{\mathrm{m}}\frac{w^2}{\Delta x} \qquad \text{(A1–A7)}$$

where K_{ij} is the force on node i when node j is displaced by one unit and all other nodes, including node i, have zero displacement.

References

Beyerlein, I.J., Phoenix, S.L., 1996. Stress concentrations around multiple fiber breaks in an elastic matrix with local yielding or debonding using quadratic influence superposition. J. Mech. Phys. Solids 44, 1997–2039.

Beyerlein, I.J., Phoenix, S.L., 1997. Statistics of fracture for an elastic notched composite lamina containing Weibull fibers—Part I. Features from Monte-Carlo simulation. Eng. Frac. Mech. 57, 241–265.

Cook, R.D., Malkus, D.S., Plesha, M.E., 1974. Concepts and Applications of Finite Element Analysis, 3rd ed. John Wiley and Sons.

Cox, H.L., 1952. The elasticity and strength of paper and other fibrous materials. Br. J. Appl. Phys. 3, 72–79.

Cox, B.N., Carter, W.C., Fleck, N.A., 1994. A binary model of textile composites—I. Formulation. Acta Metall. Mater. 42, 3463–3479.

Curtin, W.A., 1991. Theory of mechanical properties of ceramic matrix composites. J. Am. Ceram. Soc. 74, 2837–2845.

Du, Z.-Z., McMeeking, R.M., 1995. Creep models for metal matrix composites with long brittle fibers. J. Mech. Phys. Solids 43, 701–726.

Hedgepeth, J.M., 1961. Stress concentrations in filamentary structures. NASA TN D-882.

Hedgepeth, J.M., van Dyke, P., 1967. Local stress concentration in imperfect filamentary composite materials. J. Compos. Mater. 1, 294–310.

Hui, C.-Y., Phoenix, S.L., Ibnabdeljalil, M., 1995. An exact closed form solution for fragmentation of Weibull fibers in a single filament composite with applications to fiber-reinforced ceramics. J. Mech. Phys. Solids 43, 1551–1585.

Irons, B.M., 1996. Engineering applications of numerical integration in stiffness methods. AIAA J. 4, 2035–2037.

Kelley, A., Tyson, W., 1965. Tensile properties of fiber/reinforced metals: copper/tungsten and copper/molybdenum. J. Mech. Phys. Solids 13, 329–350.

Landis, C.M., McMeeking, R.M., 1998. A shear lag model for a broken fiber embedded in a composite with a ductile matrix. Comp. Sci. Technol. (to appear).

Landis, C.M., McGlockton, M.A., McMeeking R.M., 1998. An improved shear lag model for broken fibers in composites. J. Compos. Mater. (to appear).

Nairn, J.A., 1997. On the use of shear-lag methods for analysis of stress transfer in unidirectional composites. Mechanics of Materials 26, 63–80.

Nedele, M.R., Wisnom, M.R., 1994. Three-dimensional finite element analysis of the stress concentration at a single fibre break. Comp. Sci. Technol. 51, 517–524.

Phoenix, S.L., Sexsmith, R.G., 1972. Clamp effects in fiber testing. J. Comp. Mat. 6, 322–337.

Phoenix, S.L., Ibnabdeljalil, M., Hui, C.-Y., 1997. Size effects in the distribution for strength of brittle matrix fibrous composites. Int. J. Solids Structures 34, 545–568.

Press, W.H., Teukolsky, S.A., Vettering, W.T., Flannery, B.P., 1992. Numerical Recipes in Fortran 2nd Ed. Cambridge University Press, pp. 779–783.

Sastry, A.M., Phoenix, S.L., 1993. Load redistribution near non-aligned fiber breaks in a two dimensional unidirectional composite using break influence superposition. J. Mater. Sci. Lett. 12, 1596–1599.

Schwietert, H.R., Steif, P.S., 1990. A theory for the ultimate strength of a brittle-matrix composite. J. Mech. Phys. Solids 38, 325–343.

Thouless, M.D., Evans, A.G., 1988. Effects of pull-out on the mechanical properties of ceramic-matrix composites. Acta Metall. 36, 517–522.

Wagner, H.D., Amer, M.S., Schadler, L.S., 1996. Fiber interactions in two dimensional composites by micro-Raman spectroscopy. J. Mater. Sci. 31, 1165–1173.